The University of Reading

A singular vector perspective of 4D-Var: The spatial structure and evolution of baroclinic weather systems

C. Johnson
National Center for Atmospheric Research, Boulder CO, USA

B.J. Hoskins, N.K.Nichols
School of Mathematics, Meteorology and Physics, The University of Reading, Whiteknights, Reading UK

and

S.P. Ballard
Met Office, JCMM, Earley Gate, Reading UK

NUMERICAL ANALYSIS REPORT 4/05

Department of Mathematics

Abstract

The extent to which Four-Dimensional Variational data assimilation (4D-Var) is able to use information about the time-evolution of the atmosphere to infer the vertical spatial structure of baroclinic weather systems is investigated. General results are derived using the singular value decomposition of the 4D-Var observability matrices in an idealized Eady model setting. These results are confirmed with 4D-Var analyses.

The results show that 4D-Var performs well at correcting the errors that would otherwise rapidly corrupt a forecast. However, in a few cases, 4D-Var may add a rapidly growing error instead of correcting a decaying error. The ability to extract the time-evolution information can be maximized by placing the observations as far apart as possible in time, and the specification of the case-dependent background error variances is crucial in being able to project the observational information onto analysis increments that lead to the appropriate growth rate.

1. Introduction

The dynamical instability of the atmosphere means that small perturbations that are introduced into the flow may grow rapidly. For example, the flow at mid-latitudes is baroclinically unstable due to the vertical shear associated with the meridional temperature gradient. This wave-instability provides the dominant mechanism for disturbances to develop into mid-latitude weather systems. In such development, the vertical spatial structure of the disturbance plays a fundamental role in governing the development. For example, the normal-mode analysis of simple linear models (Charney, 1947; Eady, 1949) showed that the fastest growing structure exhibits a westward tilt with height in the pressure field. This vertical tilt leads to a process known as self-development where the upper and lower level waves act to intensify each other, leading to e

tional data assimilation (4D-Var) (Rabier et al., 2000) and Ensemble Filters (Evensen, 1994; Tippett et al., 2003; Lorenc, 2003a,b) extend this method by using a forecast model to link together observations that are distributed in time and also to evolve the background error covariance matrix (Lorenc, 1986). This means that observations are combined with dynamically evolved covariances so that 4D-Var is able to generate the vertical structures that are needed for baroclinic growth. For example, single observation experiments by Thépaut et al. (1996) showed that 3D-Var analysis increments do not exhibit any tilt with height, whereas 4D-Var analysis increments are anisotropic and also exhibit a westward tilt with height. Idealized experiments by Rabier and Courtier (1992) showed that 4D-Var is able to combine the information provided by the model dynamics with observations of only the eddy part of the flow to reconstruct a baroclinic wave.

Thépaut et al. (1996) demonstrated a strong link between the dominant singular vectors of the tangent linear model and 4D-Var analysis increments. Theoretical studies by Pires et al. (1996) and Rabier et al. (1996) also showed that the 4D-Var cost function is most sensitive to analysis increments given by the dominant singular vectors. Hence 4D-Var should provide accuracy of the unstable components of the flow by correcting the components in the initial errors that are rapidly growing.

Many of the previous 4D-Var studies have considered observations given at only the end of the window. However, one of the major advantages of 4D-Var is that it is able to use the model dynamics to link together a time-sequence of observations. This extra information can be used to build a

forecasts of baroclinic weather systems and also to correct errors in the initial conditions that result in rapid growth. For a complete assessment of whether 4D-Var is able to generate the appropriate vertical structures, we investigate whether 4D-Var is able to generate the appropriate structures for both baroclinic growth and decay.

The 2D Eady model is used throughout this paper. This linear model is one of the most simple models of baroclinic instability, and allows a clear understanding of the operation of 4D-Var. The 4D-Var algorithm, singular vector technique and Eady model are described in section 2. In section 3, we compare cases with growing and decaying modes and investigate the impact of the accuracy of the observations, the temporal position of the observations in the assimilation window and the position of the observations in the spatial domain. The experiments in section 3 only consider errors that result in modal growth or decay but the experiments in section 4 also consider cases with errors that result in non-modal growth. These final experiments are used to investigate the impact of the specified error variances on the growth rate of the following forecast. The main conclusions are given in section 5, and the paper then ends with a discussion. Further studies associated with this work may be found in Johnson (2003)

cost function,

$$J(\mathbf{x}_0) = \mu^2(\mathbf{x}_0 - \mathbf{x}^b)^T\mathbf{B}^{-1}(\mathbf{x}_0 - \mathbf{x}^b) + \sum_{i=0}^{N}(\mathbf{y}_i - \mathbf{H}_i\mathbf{x}_i)^T\mathbf{R}_i^{-1}(\mathbf{y}_i - \mathbf{H}_i\mathbf{x}_i), \tag{1a}$$

subject to the linear model constraint,

$$\mathbf{x}_{i+1}$$

observations, $\hat{\mathbf{y}} = \left[\mathbf{y}_0^T, \mathbf{y}_1^T, \ldots, \mathbf{y}_N^T\right]^T$, to the initial state vector, $\mathbf{x}_0$, and is denoted by

$$\hat{\mathbf{H}} = \begin{bmatrix} \mathbf{H}_0^T & (\mathbf{H}_1\mathbf{M}(t_1,t_0))^T & \ldots & (\mathbf{H}_N\mathbf{M}(t_N,t_0))^T \end{bmatrix}^T. \tag{2}$$

Then the observability matrix $\widetilde{\mathbf{H}}$ and its associated singular value decomposition is given by

$$\widetilde{\mathbf{H}} = \hat{\mathbf{R}}^{-1/2}\hat{\mathbf{H}}\mathbf{B}^{1/2} = \sum_{j=1}^{r} \lambda_j \mathbf{u}_j \mathbf{v}_j^T. \tag{3}$$

The singular values, left singular vectors (LSVs), right singular vectors (RSVs) and rank of the observability matrix are denoted by λ_j, $\mathbf{u}_j$, $\mathbf{v}_j$ and r.

The RSVs form an orthonormal basis in the uncorrelated state space, which means that the 4D-Var analysis increments can be written as:

$$\mathbf{x}^a - \mathbf{x}^b = \sum_{j=1}^{r} f_j c_j \mathbf{B}^{1/2}\mathbf{v}_j, \tag{4a}$$

where

$$f_j = \frac{\lambda_j^2}{\mu^2 + \lambda_j^2}, \tag{4b}$$

$$c_j = \frac{\mathbf{u}_j^T \hat{\mathbf{R}}^{-1/2}\hat{\mathbf{d}}}{\lambda_j}. \tag{4c}$$

and where $\hat{\mathbf{d}} = \hat{\mathbf{y}} - \hat{\mathbf{H}}\mathbf{x}^b$ is the generalized innovation vector. The RSVs are independent of the observed values and the background state. They give the possible spatial structures that can be analysed by 4D-Var for the specified linear model dynamics, linearization trajectory, error covariances and observation locations in both space and time.

The particular combination of RSVs that are included in the analysis increment is determined by the coefficients, c_j. If the vector $\hat{\mathbf{R}}^{-1/2}\hat{\mathbf{d}}$ has a large projection onto the LSV $\mathbf{u}_j$, then the corresponding RSV is given a large weight. The observational noise can have a large projection onto the LSVs with small singular values so that the corresponding RSVs would dominate the analysis increment. However, these are filtered by the filter factors, f_j, which damp the RSVs with small singular values,

$\lambda_j^2 << \mu^2$. Hence the algorithm selectively filters unrealistic structures and the analysis increment is dominated by the RSVs with large singular values.

c. Eady model

The non-dimensional equations for the 2D Eady model (Eady, 1949) are now described. The basic state is given by a linear zonal wind shear with height in a domain between two rigid horizontal boundaries. The domain is infinite in the meridional direction and the only dependence on this direction is the uniform meridional temperature gradient which is in thermal wind balance with the zonal wind shear. The density, static stability and Coriolis parameters are all taken to be constants.

The perturbation to the basic state is described by the non-dimensional buoyancy, b, on the upper and lower boundaries and by the non-dimensional quasi-geostrophic potential vorticity (QGPV), q, in the interior. Equivalently, the perturbation may also be described by the non-dimensional geostrophic streamfunction, ψ, which satisfies:

$$\frac{\partial^2\psi}{\partial x^2} + \frac{\partial^2\psi}{\partial z^2} = q, \qquad \text{in } z \in \left[-\frac{1}{2}, \frac{1}{2}\right], \qquad x \in [0, X], \tag{5a}$$

$$\frac{\partial\psi}{\partial z} = b, \qquad \text{on } z = \pm\frac{1}{2}, \qquad x \in [0, X], \tag{5b}$$

where x is the non-dimensional distance in the zonal direction, and z is the non-dimensional height. The non-dimensional time will be denoted by t. The perturbation to the basic state is advected zonally by the basic shear flow as described by the non-dimensional QG thermodynamic equation and QGPV equation:

$$\left(\frac{\partial}{\partial t} + z\frac{\partial}{\partial x}\right) b = \frac{\partial\psi}{\partial x}, \qquad \text{on } z = \pm\frac{1}{2}, \qquad x \in [0, X], \tag{6a}$$

$$\left(\frac{\partial}{\partial t} + z\frac{\partial}{\partial x}\right) q = 0, \qquad \text{in } z \in \left[-\frac{1}{2}, \frac{1}{2}\right], \qquad x \in [0, X]. \tag{6b}$$

The perturbation is periodic in the horizontal so that the lateral boundary conditions are: $b(0, z, t) = b(X, z, t)$ and $q(0, z, t) = q(X, z, t)$. The model is discretized using 11 vertical levels for QGPV with 40 grid points in one periodic interval in x. The advection equations are discretized using a

leap-frog advection scheme. The computational details to compute the 4D-Var analysis and the SVD are identical to those in JHN.

Dimensional values for x, z and t will be used to discuss the results. These are based on a domain height of $10km$, buoyancy frequency $N = 10^{-2}s^{-1}$, Coriolis parameter $f = 10^{-4}s^{-1}$. The difference in the basic state zonal wind

the QGPV

wave is inferred than for the growing mode. In both the amplitude and phase error cases, 4D-Var is much better able to correct the unobserved upper boundary wave for the case where the true state, and hence the background state error results in growth rather than decay.

These experiments illustrate that 4D-Var is able to use the time-evolution information to correct the upper level wave. However, it is not clear why 4D-Var is better at correcting the growing errors than the decaying errors, and how the analyses can be improved.

In the following experiments the SVD framework is first employed to consider further the extent to which 4D-Var is able to correct the upper level wave and produce an analysis with the correct growth rate. The concepts that are learned from the SVD framework are then confirmed by 4D-Var analyses. The analyses are verified by comparing the behaviour, including the magnitude and phase error, over the following forecast interval. The magnitude is evaluated using the non-dimensional kinetic energy (KE) norm:

$$KE = \iint v^2 dx dz \tag{7}$$

where $v = \partial\psi/\partial x$ is the perturbation meridional wind. The phase error is evaluated using the correlation between the streamfunction fields of the analysis and the true state. The error-correlation takes a value of one when the analysis is completely in phase with the true state and takes a value of minus one when they are completely out of phase.

We first consider the impact of the accuracy of the observations by varying the value of μ^2; we then examine the impact of the temporal position of the observations by varying the time of the first set of observations; and we finally examine the impact of the spatial position of the observations by observing horizontal lines of the buoyancy field at different heights.

c. Accuracy of the observations

The ability of 4D-Var to reconstruct the upper level wave for different values of μ^2 is now examined. The observations are again of the lower level buoyancy at the beginning and the end of the window, but the value of μ^2 is varied. It is assumed that in the appropriate value of μ^2 is used in the assimilation of real data. A large value of μ^2 implies that relatively inaccurate observations are assimilated

observations are assimilated and so the analysis is close to the true state. Hence varying the size of μ^2 allows us to investigate the impact of the accuracy of the observations.

1). SVD RESULTS

We first examine the RSVs of the observability matrix and discuss [illegible] conclusions

increase in the amplitude of the wave

the second pair of RSVs, with $\lambda = 0.74$, contain the information needed to reconstruct the state in the unobserved regions and also to give a decaying decaying a3992 1 47.1598 0 Td(0j0 0 -0.1 216.80 Td(decayi

with the growing mode.

There are similar results for the cases where the background state has a phase error. For both the growing and decaying modes, the KE values for the background state are identical to those for the true state (Fig. 6). The error can only be seen in the error correlation values (Fig. 7). For the growing mode, when $\mu^2 = 0.1$, both pairs of RSVs contribute to the analysis increment, and both the phase and KE are close to the true state. When $\mu^2 = 1$, only the first pair of RSVs contribute to the analysis increment. This acts to correct the lower level wave, but not the

1). SVD RESULTS

Singular value decompositions of the corresponding observability matrices are first considered. For a fixed assimilation window length, the temporal position of the initial observations has very little impact on the spatial structure of the RSVs and so their structures are not shown. There is, however, a change in the singular values. Fig. 8 shows the singular values of the first and second pairs of RSVs that contribute to the analysis increment as selected by the values of c_j (not necessarily always numbers $2\&3$ and $6\&7$). When the initial observations are at T+0, the singular values are $\lambda = 2.99$ and 0.74. These correspond to the RSVs shown in Figs. 3 and 4. When the initial observations are at T+6 the singular values are $\lambda = 6.44$ and 0.74. For the T

2). 4D-VAR ANALYSES

4D-Var analyses using observations of the lower level buoyancy but at different times are now compared. The first set of observations are given at the be

the beginning of the window are also important.

e. Spatial position of the observations

The impact of the spatial position of the observations is considered by repeating the SVD analysis and 4D-Var experiments with the horizontal line of observations given at different heights. This is achieved by observing the interior non-dimensional buoyancy, which is the vertical derivative of the non-dimensional streamfunction. The observations in each case are given at the beginning and the end of a 12h assimilation window.

1). SVD RESULTS

The singular values of the first and second pairs of RSVs, as a function of the height of the buoyancy observations, are shown in Fig. 12. Due to the symmetry of the of the Eady model, the experiments using observations on the lower boundary are equivalent to those using observations on the upper boundary. Hence, the curves are symmetrical about 5km. As the height of the observations is increased from 0 to 4.5km, the singular values of both the first and second RSVs decrease. The former decreases from 2.99 to 1.64 and the latter from 0.74 to 0.57.

The SVD shows that we expect the 4D-Var analyses to be closest to the truth when the observations are nearest to the upper or lower boundaries, as these give the largest singular values. The normal modes are driven from the boundaries and their buoyancy fields have their largest amplitudes at the boundaries. Hence observing the boundary buoyancy could be expected to be optimum and the difference between the observations and the background state is largest at the boundaries. Therefore, more accurate information can be extracted in the presence of relatively noisy observations when the observations are closest to the relevant boundary, here the lower one. This is now confirmed with the actual 4D-Var analyses.

2). 4D-VAR ANALYSES

When the true state is given by the growing mode, the variance ratio is specified as $\mu^2 = 10$. With this value, the position of the observations has the most impact on the filtering of the first pair of

RSVs. When the height of the observations is increased, the first pair of RSVs are filtered more. The KE values (Fig. 13a) show that the analysis is indeed closest to the background state when the observations are near to the centre of the domain and close to the true state when the observations are on the lower boundary.

When the true state is given by the decaying mode, the variance ratio is specified as $\mu^2 = 0.1$. With this value, the position of the observations has the most impact on the filtering of the second pair of RSVs. When the height of the observations is increased, the second pair of RSVs are filtered more so that the first pair dominate the solution, leading to growth instead of decay. The KE values (Fig. 13b) show that the best analysis is indeed obtained when the observations are on the lower boundary.

.

in which this can occur. First, as the accuracy of the observations increases, the value of μ^2 decreases. Second, as the time between the initial and final sets of observations increases, the singular value of the second pair of RSVs increases. Third, as the line of buoyancy observations is moved from the centre of the domain to either the upper or lower boundary, the singular values of both the first and second pairs of RSVs increases.

4. Results considering modal and non-modal growth

The experiments in section 3 are based on background state errors that are given by either a growing or decaying normal mode. Such experiments are useful for understandingo

matrices are given in Appendix A. To simplify the experiments, we consider the case where all the background state values are zero, $\mathbf{x}^b = 0$. The cost function is then given by:

$$J(\mathbf{x}_0) = \mathbf{x}_0^T \begin{pmatrix} \mu_b^2 \mathbf{B}_{bb} & 0 \\ 0 & \mu_q^2 \mathbf{B}_{qq} \end{pmatrix} \mathbf{x}_0 + \left(\hat{\mathbf{y}} - \hat{\mathbf{H}}\mathbf{x}_0\right)^T \left(\hat{\mathbf{y}} - \hat{\mathbf{H}}\mathbf{x}_0\right) \tag{8}$$

The true state is given by either the most rapidly growing normal mode or a PV-dipole that exhibits non-modal growth, the equations for which are given in Appendix A. The horizontal domain is increased to 8000km, with 80 grid points in the horizontal. Horizontal lines of perfect observations of the non-dimensional buoyancy are given at the beginning and the end of a 6h window at a height of 4.5km. Providing observations in the middle of the spati
inp 31.32 1.32-loq5Tj 31.67is1.32-loTm(matricesnTj 8.51997 (
2 4560.3 25tl

b. SVD

The spatial structures of the analyses are shown at the beginning of the window. We first consider cases where the true state is given by the growing normal mode. The true state, shown in Fig. 15a, is given by buoyancy waves and zero interior QGPV. This gives an exponential KE growth rate, shown in Fig. 16a, that is constant throughout the forecast period. The analyses using the three different variance ratio specifications are shown in Fig. 15. For specification 1, a large analysis increment (amplitude $3.$) is added to the buoyancy fields and a small analysis increment (amplitude 10^{-4}) is added to the interior QGPV. This

cases using the 2D Eady model with a single horizontal line of buoyancy observations at two times during the assimilation period have been investigated. The SVD provides a general framework, without the need for repeating numerous 4D-Var identical twin experiments. However, to confirm the anticipated results from the SVD, we have also examined many 4D-Var analyses and compared the evolution of the KE values and the correlation of the streamfunction field throughout the assimilation window and following forecasts.

Three main conclusions from this work can be drawn. First, we have shown that 4D-Var preferentially generates an analysis increment that leads to growth, but a decaying analysis increment can be generated provided that the information about the evolution can be extracted from the observations. Second, the ability of 4D-Var to extract the valuable time-evolution information can be maximized by adjusting the locations of the observations in space and time. Third, the specification of the appropriate background error covariances is crucial in being able to generate analysis increments that lead to the appropriate growth rate.

6. Discussion

The fact that 4D-Var is efficient in correcting rapidly growing errors is not a new result. Previous studies by Thépaut et al. (1996); Pires et al. (1996) and Rabier et al. (1996) demonstrated that a 4D-Var algorithm with no background term is able to use observations given at the end of the assimilation window to correct such errors. However, this paper has extended this conclusion to show that 4D-Var is more efficient in correcting such errors when information about the time-evolution of the observed system can be inferred. Further, we have shown that in the case where the actual errors are decaying, [illegible]

APPENDIX A

Definitions of the true state initial conditions and background error correlation matrices

The normal modes are defined (e.g. Hoskins and Bretherton, 1972) as:

$$\psi(x,z) = \cosh(kz)\cos(kx) - \alpha\sinh(kz)\sin(kx), \qquad \text{Growing Mode} \qquad \text{(A.1a)}$$

$$\psi(x,z) = \cosh(kz)\cos(kx) + \alpha\sinh(kz)\sin(kx), \qquad \text{Decaying Mode} \qquad \text{(A.1b)}$$

where $k = 1.6$, $\alpha = 2.\ 9$ and the interior QGPV is zero.

APPENDIX B

On the use of perfect observations

The experiments in this paper use perfect observations rather than observations with errors, but still include the effect of filtering provided by the background term in the cost function. We now describe, first theoretically and then with experiments, why these results are relevant to assimilation with real data. The effects of observational noise and filtering by 4D-Var are described in further detail in JHN.

Following from (4), when imperfect observations $\hat{\mathbf{y}}^{\varepsilon} = \hat{\mathbf{H}}\mathbf{x}^t + \boldsymbol{\varepsilon}$ are assimilated, the analysis increments can be written in terms of components from the true signal $\hat{\mathbf{H}}\mathbf{x}^t$ and the observational noise $\boldsymbol{\varepsilon}$.

$$\mathbf{B}^{-1/2}(\mathbf{x}^a - \mathbf{x}^b) = \sum_j f_j c_j^t \mathbf{v}_j + \sum_j f_j c_j^{\varepsilon} \mathbf{v}_j \tag{B.1a}$$

where

$$c_j^t = \mathbf{u}_j^T \mathbf{R}^{-1}(\hat{\mathbf{H}}\mathbf{x}^t - \hat{\mathbf{H}}\mathbf{x}^b)/\lambda_j \tag{B.1b}$$

$$c_j^{\varepsilon} = \mathbf{u}_j^T \mathbf{R}^{-1}\boldsymbol{\varepsilon}/\lambda_j \tag{B.1c}$$

Typically, the observational noise has a large projection, c_j^{ε}, onto the RSVs with small spatial scales and associated with small singular values, whilst the true signal, c_j^t, has a large projection onto the RSVs with large spatial scales and associated with large singular values. This is illustrated in Fig.B.1. The role of the filter factor, f_j, is to filter the contribution from the noise whilst retaining the contribution from the true signal. When the appropriate value for the variance ratio is specified, the contribution from the noise, $\sum_j f_j c_j^{\varepsilon} \mathbf{v}_j$ (the second term in equation B.1a), should be close to zero so that the equations for perfect and imperfect observations are almost identical. This means that the analysis with perfect observations should be close to the analysis with imperfect observations. Thus the relevance of perfect observations relies on the assumption that the observational noise is projected onto the RSVs with small singular values and therefore that the noise is filtered from the

solution. It is only with this same assumption that variational assimilation methods can be of use.

The analysis with perfect observations does account for the fact that the observational noise is filtered, because the appropriate amount of filtering is also applied to the true signal. This is very different to a similar analysis with perfect observations but with no background term and hence no filtering.

There may be some small differences between the analyses for perfect and imperfect observations as it is possible for the observational noise to project onto the RSVs with large singular values. These small differences will depend on the actual observational errors and are likely to become important for a series of assimilation windows in which the forecasts become the background states for the next analysis. However, for a single assimilation window it is unlikely that these differences have a significant impact on the results. Further, as these differences depend on the structure of the observational noise, an ensemble of experiments, with different values for the random noise, would be needed to deduce concrete conclusions. The use of perfect observations eliminates this need.

To finally confirm that the results with perfect observations are almost equivalent to those with imperfect observations, we compare an analysis that uses perfect observations with an analysis that uses noisy observations. The true state is given by a growing mode and the background state has a phase error. The case with noisy observations has random noise added to the perfect observations that has a Gaussian distribution with standard deviation 1.5. The appropriate value of μ^2, and hence the appropriate amount of filtering, is found by repeating the analyses with different values of μ^2

List of Tables

List of Figures

13 The evolution of the

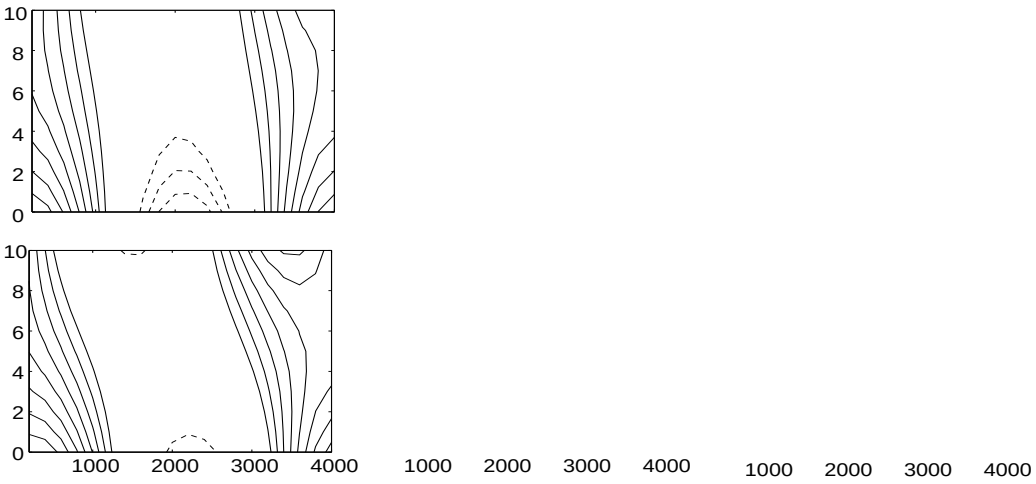
10
8
6
4
2
0
10
8
6
4
2
0
1000
2000
3000
4000
1000
2000
3000
4000
1000
2000
3000
4000

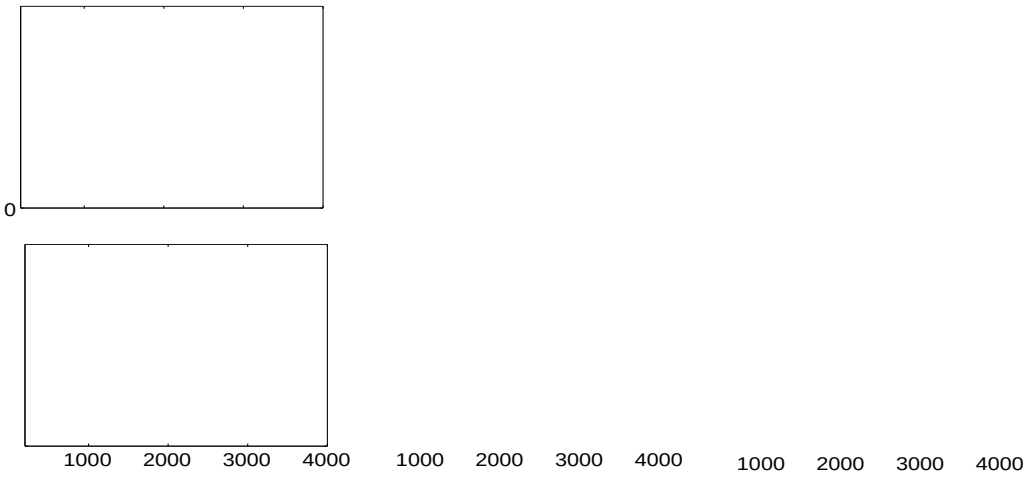
0
1000
2000
3000
4000
1000
2000
3000
4000
1000
2000
3000
4000

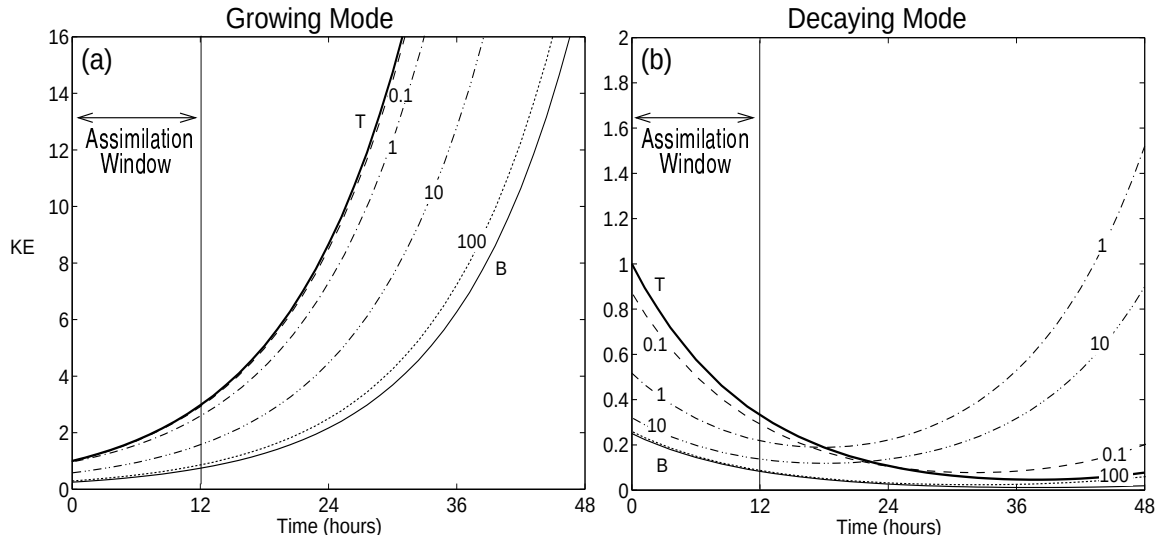

Figure 5: The evolution of the kinetic energy (KE) for the cases where the background state has an amplitude error and the true state is given by the most rapidly (a) growing and (b) decaying mode. The true state KE is shown by the thick solid line (T) and the background state KE is shown by the thin solid line (B). The analyses have specified error variance ratios μ^2 of 0.1 (dash), 1 (dot-dash), 10 (dot-dot-dash) and 100 (dot).

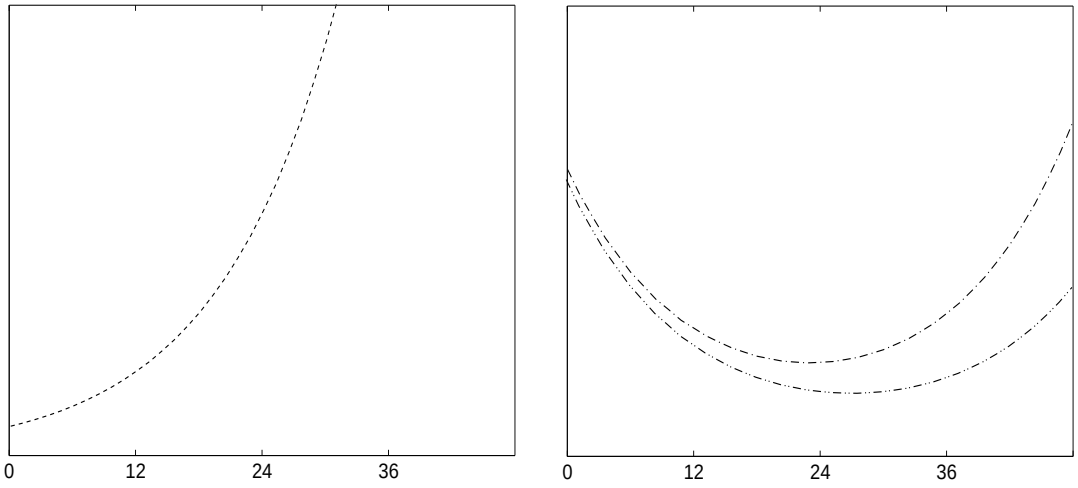
0
12
24
36
0
12
24
36

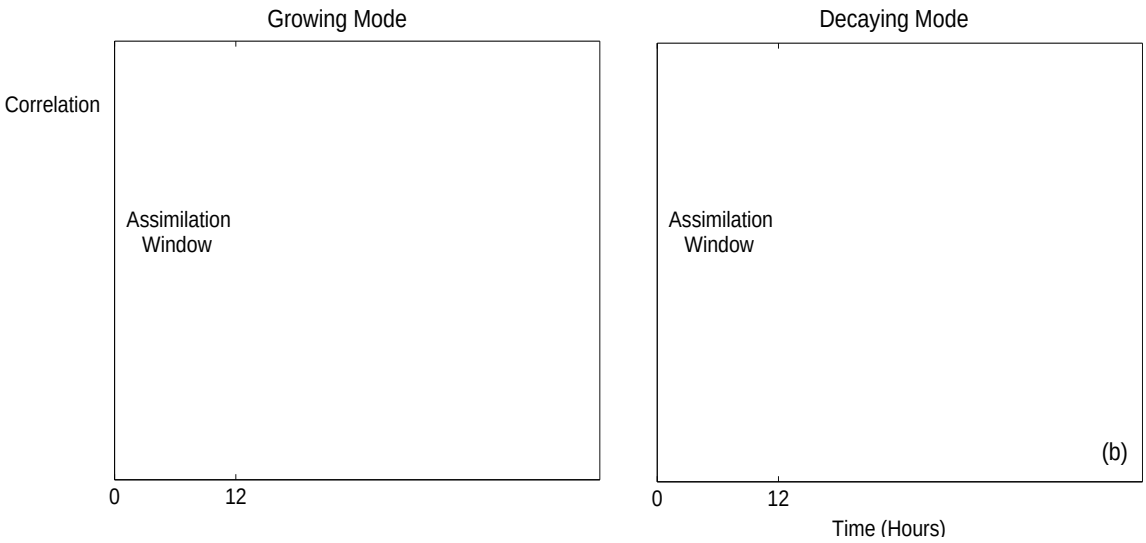
Growing Mode
Decaying Mode
Correlation
Assimilation
Window
Assimilation
Window
(b)
0
12
0
12
Time (Hours)

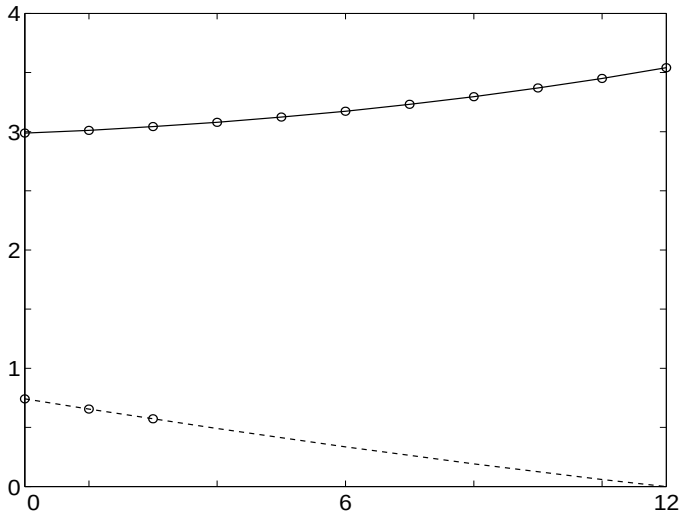
4
3
2
1
0
0
6
12

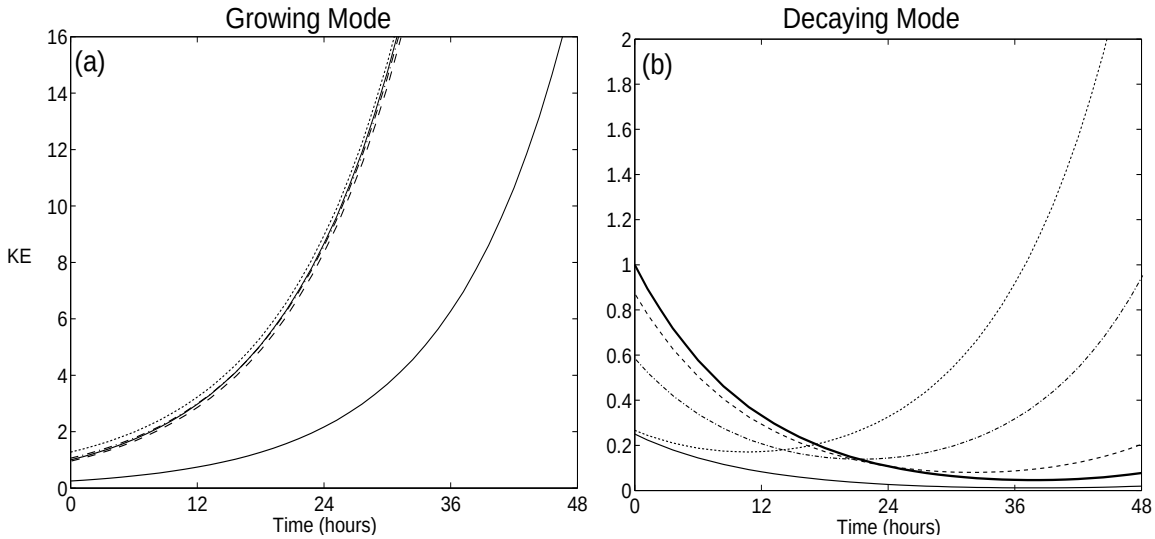
Growing Mode
(a)
KE
Time (hours)
Decaying Mode
(b)
Time (hours)

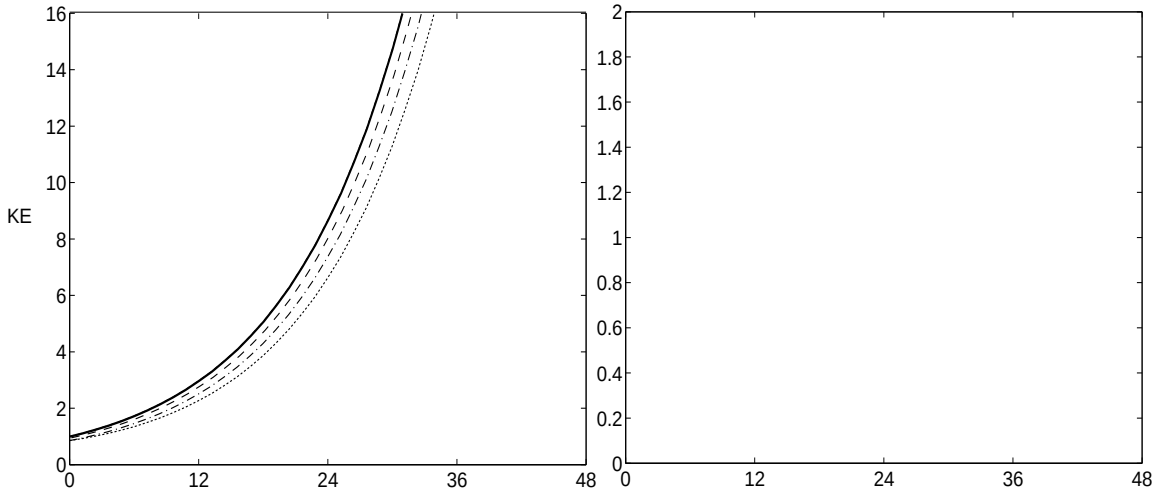
KE
16
14
12
10
8
6
4
2
0
0
12
24
36
48
2
1.8
1.6
1.4
1.2
1
0.8
0.6
0.4
0.2
0
0
12
24
36
48

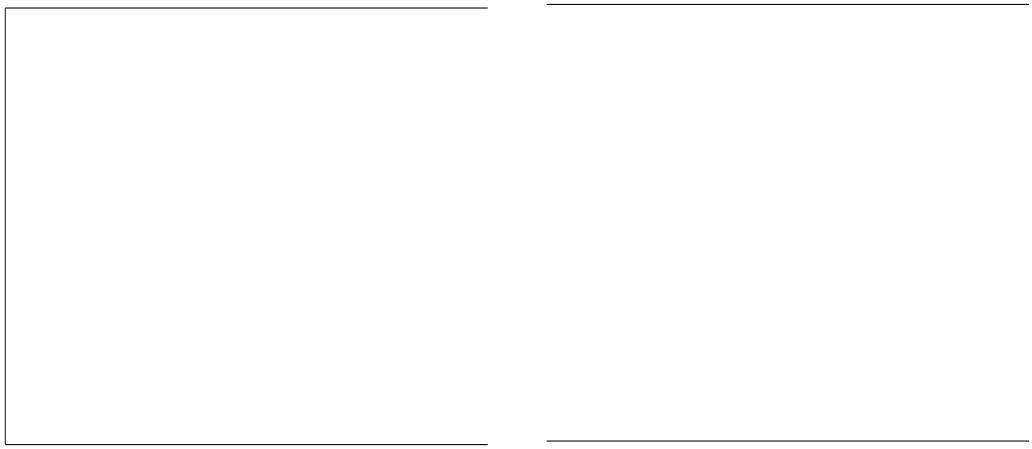

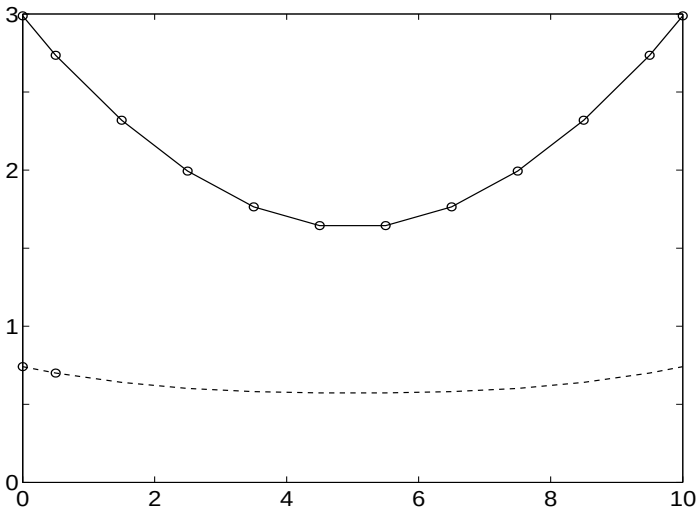
3
2
1
0
0
2
4
6
8
10

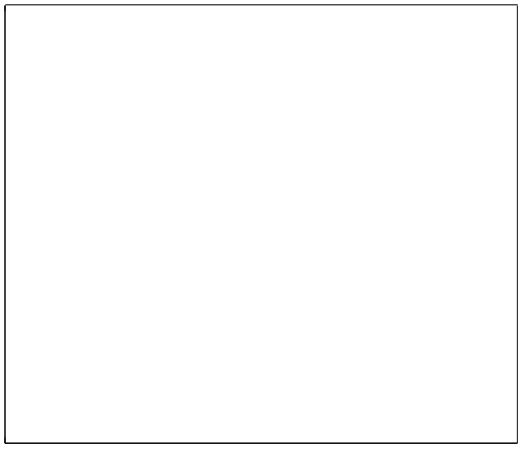

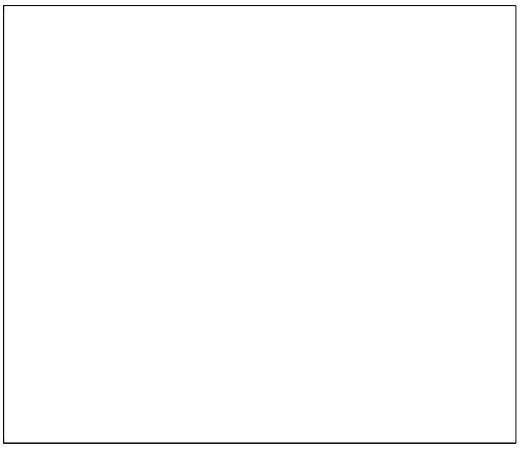

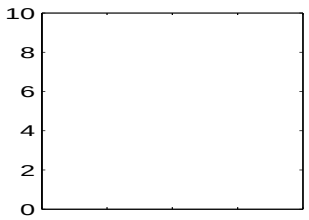
10
8
6
4
2
0

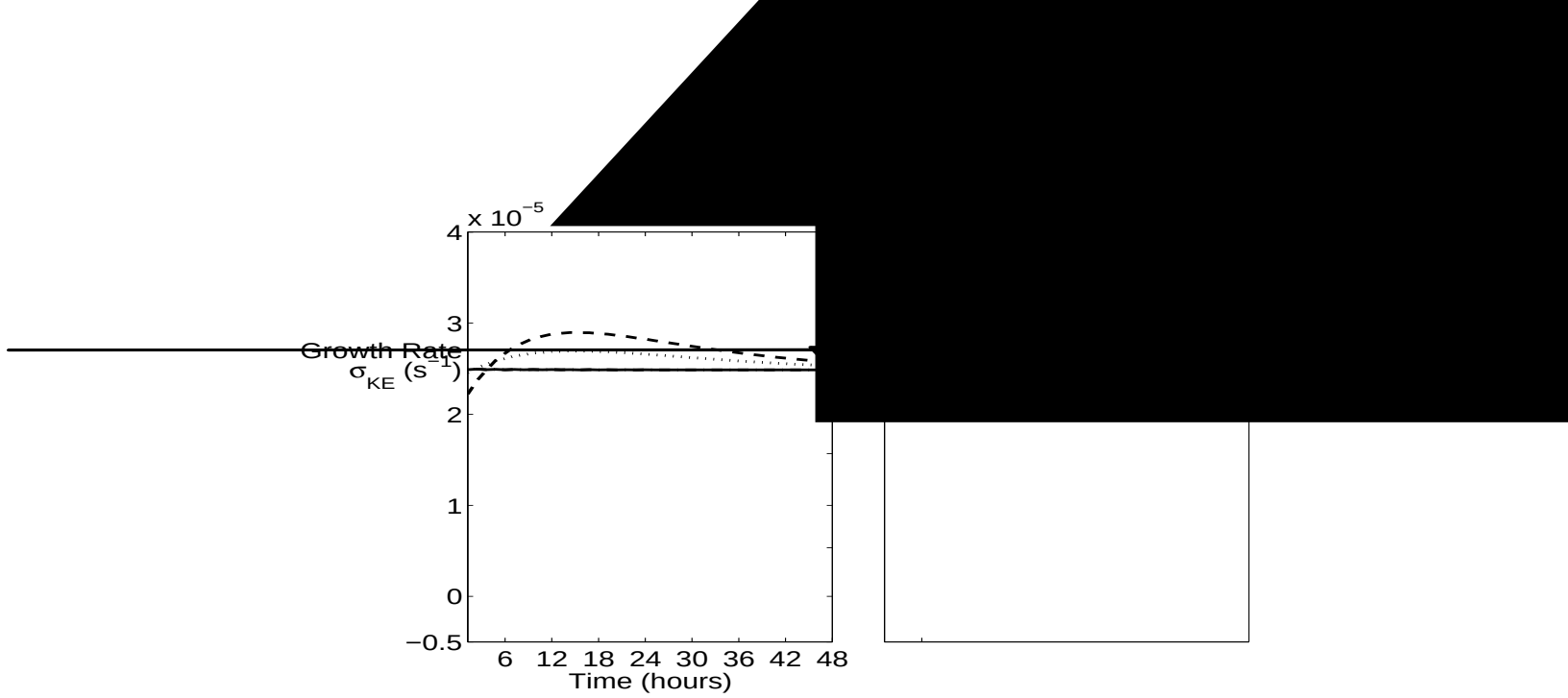
x 10^−5
4
3
2
1
0
−0.5
Growth Rate
σ_KE (s^−1)
6 12 18 24 30 36 42 48
Time (hours)

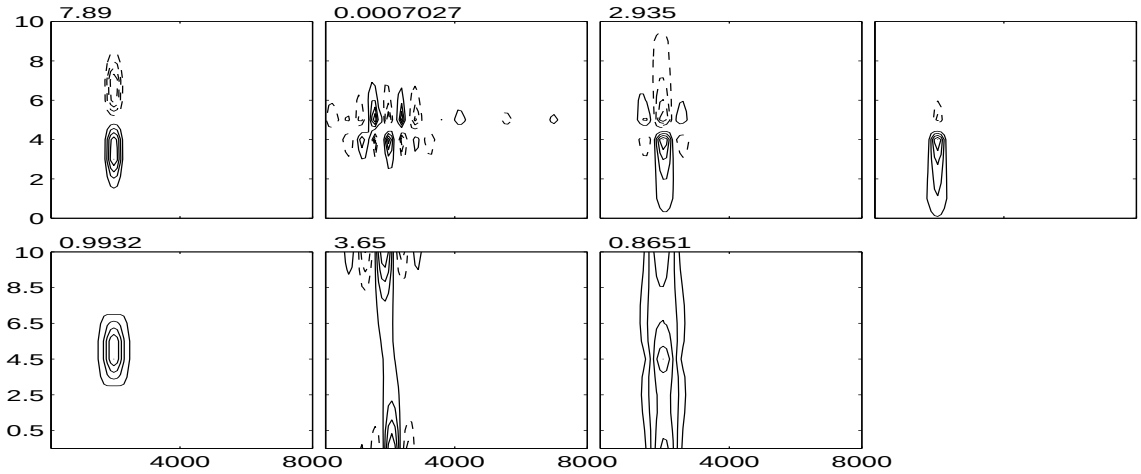
7.89
0.0007027
2.935
0.9932
3.65
0.8651
10
8
6
4
2
0
10
8.5
6.5
4.5
2.5
0.5
4000
8000
4000
8000
4000
8000

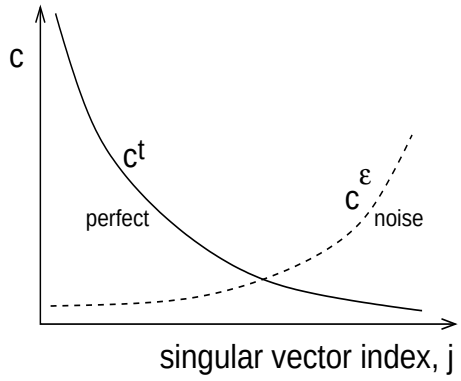
c
c^t
perfect
c^ε
noise
singular vector index, j

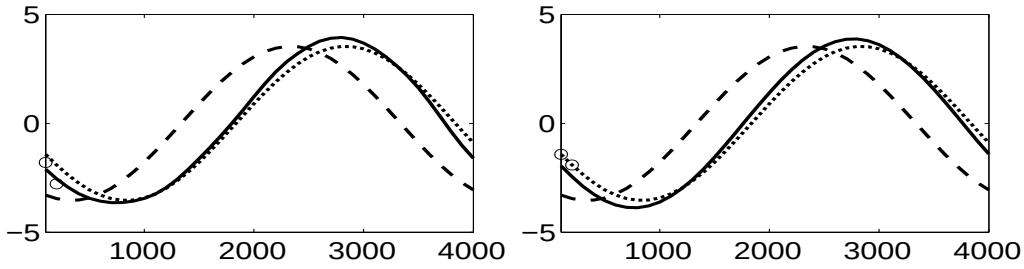
5
0
−5
1000
2000
3000
4000
5
0
−5
1000
2000
3000
4000